LUND UNIVERSITY

Snow cover and snow albedo changes in the central Andes of Chile and Argentina from daily MODIS observations (2000–2016)

Malmros, Jeppe K.; Mernild, Sebastian H.; Wilson, Ryan; Tagesson, Torbern; Fensholt, Rasmus

1   **Snow cover and snow albedo changes in the central Andes of Chile and Argentina**

2   **from daily MODIS observations (2000–2016)**

3

4   JEPPE K. MALMROS, [1], SEBASTIAN H. MERNILD, [2, 3, 4], RYAN WILSON, [5],

5   TORBERN TAGESSON, [1], RASMUS FENSHOLT, [1]

6

7   [1] *Department of Geosciences and Natural Resource Management, University of Copenhagen,*
8   *Copenhagen, DENMARK*
9
10   [2] *Nansen Environmental and Remote Sensing Center, Bergen, NORWAY,*
11
12   [3] *Direction of Antarctic and Sub-Antarctic Programs, Universidad de Magallanes, Punta Arenas,*
13   *CHILE*
14
15   [4] *Faculty of Engineering and Science, Western Norway University of Applied Sciences, Sogndal,*

16   *NORWAY*

17   [5] *Department of Geography and Earth Sciences, Aberystwyth University, Aberystwyth, UK*

18

19

20

21

25

26

27

28

29

30

31   Corresponding author address:

1

32   Department of Geosciences and Natural Resource Management, University of Copenhagen, Øster

33   Voldgade 10, 1350 Copenhagen, Denmark.

34   E-mail: jkmalmros@gmail.com

Abstract

        The variables of snow cover extent (SCE), snow cover duration (SCD), and snow albedo (SAL) are primary factors determining the surface energy balance and hydrological response of the cryosphere, influencing snow pack and glacier mass-balance, melt, and runoff conditions. This study examines spatiotemporal patterns and trends in SCE, SCD, and SAL (2000–2016; 16 years) for central Chilean and Argentinean Andes using the MODIS MOD10A1 C6 daily snow product. Observed changes in these variables are analyzed in relation to climatic variability by using ground truth observations (meteorological data from the El Yeso Embalse (EYE) weather station) and the Multivariate El Niño index (MEI) data. We identified significant downward trends in both SCE and SAL, especially during the onset and offset of snow seasons. SCE and SAL showed high inter-annual variability which correlate significantly with MEI applied with a one-month time-lag. SCE and SCD decreased by an average of $\sim13 \pm 2$ % and 43 ± 20 days respectively, over the study period. Analysis of spatial pattern of SCE indicates a slightly greater reduction on the eastern side ($\sim14 \pm 2$ %) of the Andes Cordillera compared to the western side ($\sim12 \pm 3$ %). The downward SCE, SAL, and SCD trends identified in this study are likely to have adverse impacts on downstream water resource availability to agricultural and densely populated regions in central Chile and Argentina.

1. Introduction

Snow in the semi-arid mountain regions of the central Andes of Chile and Argentina provides important water resources to more than 10 million people and is of major importance for agriculture in this area (Masiokas et al. 2006). Moreover, snow constitutes a key seasonal component in the surface energy and hydrosphere budgets, reflecting incoming solar shortwave radiation (e.g., Konzelmann and Ohmura 1995). Hydrological balance in the cryosphere is highly influenced by the amount of snow precipitation and the spatiotemporal variability of seasonal snow cover extent (SCE). The combined variability of snow precipitation, SCE, and snow cover duration (SCD) directly influences river-runoff variabilities and glacier surface-mass balance conditions (Ragettli et al. 2016; Wilson et al. 2016).

On high mountain glaciers, energy availability for snow and ice melt is regulated by surface albedo which is defined as the ratio of incoming solar radiation reflected by a surface (Cuffey and Paterson 2010). Fresh snow, for example, acts as a near perfect reflector with albedo values of up to 0.98. However, snow albedo (SAL) diminishes over time as a result of snow metamorphism, decreasing to as low as 0.46 (Cuffey and Paterson 2010). Rainfall can further enhance this natural lowering of SAL through the addition of latent energy, which can initiate melting (Benn and Evans 2010) and cause downwasting and thinning of glaciers (Neckel et al. 2017). Snow and ice albedo can also be reduced by the surface deposition of dust and/or anthropogenic soot (Hansen and Nazarenko 2004; Cereceda-Balic et al. 2012). In the central Andes, an additional factor which influences SAL is the seasonal formation of penitents. Often forming in areas of low humidity and high solar elevation, snow penitents can result in significant changes in the surface roughness of snow-covered terrain, which, in turn, influences SAL and sublimation conditions (Corripio and Purves 2006).

The overall variability of SAL is influenced by a variety of factors: snow grain size, levels of contamination, solar zenith angle, cloud cover, snow metamorphism, surface roughness, age factor, and liquid water content, amongst others (Warren and Wiscombe 1980; Mernild et al. 2015a). Since SAL is a key parameter determining the amount of energy available for surface melting snow and ice, snow-sublimation, and metamorphosis, spatiotemporal variability in SAL is important when determining snow ablation conditions (Male and Granger 1981; Brock et al. 2000; Hock 2005; Gardner and Sharp 2010; Mernild et al. 2016a).

Spatiotemporal trends in SCE and SAL interpolated from point measurements often include large errors, especially in remote mountainous regions characterized by limited ground observations,

95   localized climate conditions and complex terrain. In comparison, satellite-based remote sensing and

96   satellite derived snow cover products provide opportune sources of large-scale SCE and SAL

97   measurements and have been successfully used as key inputs in climate, atmospheric and hydrological

98   models (Farr et al. 2007; Mernild et al. 2008; Vuille et al. 2008; Mernild et al. 2015a). Remote sensing

99   systems acquiring data from the visible (VIS) to shortwave infrared (SWIR) spectrum with a high

100   temporal resolution are well suited for monitoring SCE and SAL over large areas, providing good

101   spatial and temporal coverage (Wiscombe and Warren 1980; Dozier and Frew 1981; Dubayah 1992;

102   Knap et al. 1999).

103   Several remote sensing based snow cover products are currently available, most of which apply

104   either the normalized difference snow index (NDSI) (Hall et al. 1995), empirical relationship

105   assumptions or spectral un-mixing models (Klein and Stroeve 2002a). Optical sensor systems,

106   however, are unable to acquire useful information during cloudy conditions (Justice et al. 1998;

107   Marchane et al. 2015). Therefore, frequent satellite observation revisits are essential to study changes

108   in SCE and SAL, since surface conditions can vary rapidly and may change considerably over a few

109   days.

110   To compensate for extensive cloud cover, compromises are often made by conducting satellite

111   analysis based on composite products such as the MODIS (Moderate Resolution Imaging

112   Spectroradiometer) 8 day snow cover MOD10A2 product (Hall et al. 2002), which can mask subtle

113   changes in SCE and SAL over time. In order to avoid this limitation, the MODIS MOD10A1

114   Collection 6 (C6) dataset was used this study. MOD10A1 provides daily SCE and SAL values globally

115   at a spatial resolution of 500 m, making it suitable for evaluating seasonal trends in SCE and SAL (Hall

116   et al. 2002; Liang et al. 2005; Marchane et al. 2015; Hall and Riggs 2016; Saavedra et al. 2016; Li et al.

117   2017; Huang et al. 2017; Dariane et al. 2017), snow cover phenology (Xu et al. 2017) and the relation

118   between SCE and climate (Gurung et al. 2017; Li et al. 2017). Using MOD10A1 data, this study

119   analyses spatiotemporal changes in SCE and SAL in the central Andes of Chile and Argentina by

120   parameterizing a time series of seasonal SCE and SAL metrics at the per-pixel level. Furthermore, this

121   study examines the large-scale influence of ENSO events on SCE and SAL as well as the more

122   localized effect of climatic variability (utilizing meteorological data from the El Yeso Embalse (EYE)

123   weather station) and elevation.

124

2. Study area

The Andes of central Chile and Argentina (31°S and 40°S) contain some of the highest peaks of the entire Andes Cordillera, reaching altitudes above 6,000 m above sea level (a.s.l.) (Fig. 1). Covering an area of ~1,730 km^2, the study area chosen is located immediately west of Santiago de Chile (32°50'−34°50'S; 69°20' − 70°40'W). This study area includes several river basins which supply freshwater to large downstream populations (10+ million people in Chile and 2+ million in Argentina), hydro-power stations, and agricultural lands on both sides of the cordillera (Corripio and Purves 2006). This area of the central Andes also includes the largest glaciated areas in South America outside southern Patagonia (Saavedra et al. 2016). River runoff in this central region originates primarily from snowmelt (Masiokas et al. 2006), with snowfall contributing up to ~85 % of runoff from specific catchments (Mernild et al. 2016b). The availability of snow as a freshwater resource is therefore of vital socio-economic importance in this semi dry region (Peña and Nazarala 1987; Meza et al. 2012; Carey et al. 2017).

The intra-annual variability of precipitation in central Andes is highly influenced by the placement of an atmospheric high-pressure cell over the southeastern Pacific Ocean. This cell normally inhibits precipitation in the Austral summer (December − February) and allows for the passage of westerlies and frontal precipitation during Austral winters (June − August) (Garreaud et al. 2009). Precipitation events are usually concentrated between April and October, providing ~95 % of the mean annual totals, peaking in June or July (Masiokas et al. 2016). The strength of El Niño Southern Oscillation (ENSO) influences inter-annual variability in precipitation, with higher/lower precipitation occurring during El Niño/La Niña events (Rutllant and Fuenzalida 1991; Escobar et al. 1995; Leiva 1999; Montecinos and Aceituno 2003; Garreaud et al. 2009). During El Niño events, precipitation increases predominantly during the austral winter (Masiokas et al. 2006; McClung 2013). Whilst El Niño events do influence precipitation amounts, these events shows little or no significant signal in annual mass balance measurements of glaciers located in the central Andes but has been linked to the Pacific Decadal Oscillation (PDO) rather than the ENSO (Mernild et al. 2015a).

Along the central Andes, annual accumulation of snow is highest at 4,000 – 5,000 m a.s.l., where glacier accumulation zones are also present (Cornwell et al. 2016; Mernild et al. 2016b; Mernild et al. 2016c). Precipitation differences observed between the western and eastern sides of the Andes Cordillera occur due to the combination of orographic effects of the mountain relief and the dominating

westerly wind direction which results in precipitation amounts and humidity being lower on the eastern

Cordillera slopes (Cornwell et al. 2016; Mernild et al. 2016b).

For the central Andes, mean surface air temperatures are normally highest between December

and March and lowest in July and August (Masiokas et al. 2016) and temperatures in the Andes showed

increasing trends from 1975 to 2006 (~0.25°C/decade) (Falvey and Garreaud 2009). The 0°Cisotherm

for the western side of the cordillera (40 km northeast of Santiago de Chile), was located at 3,385 m

a.s.l. between 2009 and 2014 (Mernild et al. 2016c).
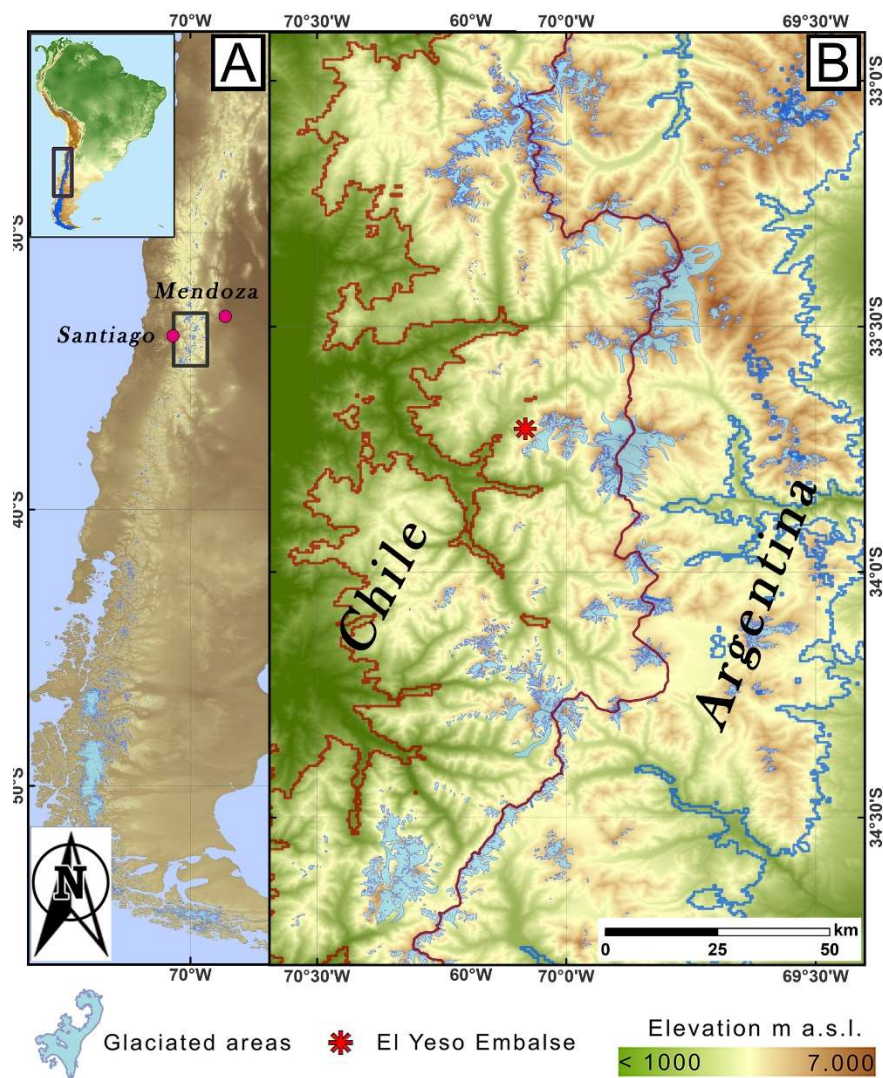
Figure 1: (a) The central Andes of Chile and Argentina; and (b) including the area of interest west and

east snow cover regions delineated by red and blue lines, respectively. The divide between the western

166   and eastern Andes also represents the natural border (continental divide) between Chile and Argentina.

167   Blue areas represents glaciers. The red star in the center of the study area represents the location of the

168   El Yeso Embalse (EYE) weather station.

169

170   **3. Data**

171

172   *3.1 MODIS data*

173   The MOD10A1 C6 (henceforth MOD10A1 unless other version is implied) snow product is

174   derived from daily data acquisitions by the MODIS sensor aboard the Terra spacecraft (Riggs et al.

175   2017). The MODIS global daily snow cover product MOD10A1 (MODIS/Terra Snow Cover Daily L3

176   Global 500m Grid) is derived from cloud free observations and is well suited for regional snow cover

177   and albedo mapping (Hall et al. 2002; Liang et al. 2005; Dozier et al. 2008; Rittger et al. 2013; Fausto

178   et al. 2015; Mernild et al. 2015b). The latest MOD10A1 product was released in the spring of 2016 and

179   includes a range of improvements to the previous version including, amongst others, the removal of

180   Terra sensor degradation issues and improvements in atmospheric calibration (Lyapustin et al. 2014).

181   Importantly, the algorithms used to compile the MOD10A1 snow product are modified to include only

182   the best quality observations from the atmospherically corrected MOD10GA product (Hall et al. 2002).

183   Individual MOD10A1 product parts include NDSI, NDSI snow cover (SCE), SAL and corresponding

184   quality control flags. The MOD10A1 NDSI SCE calculated is produced from an empirical relationship

185   with NDSI values, where NDSI values are multiplied by a constant (Dozier et al. 2008; Hall and Riggs

186   2016). By using only full snow cover pixels, the accuracy of the MOD10A1 SAL product is improved

187   in terms of ground truth comparisons (Sorman et al. 2007; Mernild et al. 2015b). The overall error of

188   the MOD10A1 SAL product can vary substantially but is found to be in the order of 1–10 % for good

189   observations with low atmospheric disturbances across the Greenland ice sheet (Klein and Stroeve

190   2002b). The overall error at this location is likely to be higher due to the complex terrain of the Andes

191   Mountains. However, changes in albedo can still be quantified and here we opted for a per-pixel

192   temporal change analysis that is expected to mitigate the influence of topography to some degree by

193   avoiding direct inter-comparison of pixels influenced by different slope/aspect.

194   MOD10A1 data used in this study was obtained from the NASA Earth Observation System

195   Data and Information System (EOSDIS) Reverb ECHO website (https://reverb.echo.nasa.gov/). Out of

the 5,844 potential scenes available between March 1 2000 and Feb 29 2016, only 121 (~2 %) were

missing in the archive, with a maximum temporal gap of 17 days. The snow cover year (season) was

set to start 1 March and end February 28 (29) based on analysis of the data set. Pixels with cloud cover

or poor retrievals were omitted as determined from QA flags and only pixels flagged as "best quality"

were included in the further analysis (see section 4.1). Out of all pixels in the data series 74.8 %

contained "best quality" data (supplementary material S1).

3.2 Ancillary data

Elevation data were obtained from the Shuttle Radar Topography Mission (SRTM) v.3. SRTM

provides elevation data at a spatial resolution of 30 meters with an overall vertical accuracy of ~10 m

and geo-position error of ~9 m (Farr et al. 2007). Multivariate El Niño index (MEI) ranks were

obtained from the National Oceanic and Atmospheric Administration (NOAA) website

(http://www.esrl.noaa.gov/psd/enso/mei/table.html). The MEI provides a ranked index of the strength

of El Niño and La Nina events. MEI values are normalized for each bimonthly season (Wolter and

Timlin 2011) and cover the 16-year study period of snow cover and snow albedo observations.

We acquired mean monthly air temperature (MMAT), mean annual air temperature (MAAT),

and monthly precipitation sums (2000–2016) from the El Yeso Embalse meteorological station (EYE)

(location in Fig. 1; data shown in supplementary material S2) from Dirección General de Aguas (DGA;

www.dga.cl). Finally, glacier outlines were obtained from the Randolph glacier inventory v. 5.0

(Pfeffer et al. 2014) in combination with updated glacier shapes from 2013/2014 (Malmros et al. 2016).

4. Methods

4.1 Time series preprocessing

The MOD10A1 time series was preprocessed and analyzed using the program TIMESAT

(Jönsson and Eklundh 2002, 2004; Eklundh and Jönsson 2015). TIMESAT originally developed to

analyze vegetation seasonality can be applied to all remote sensing data containing seasonal variability.

We applied a Savitzky-Golay filter within TIMESAT which allows for a smoothening of the

MOD10A1 time-series by applying polynomial fitting to the data points within a moving window of a

226   certain width (Savitzky and Golay 1964; Jönsson and Eklundh 2004). Missing dates were filled with

227   blank scenes before smoothing (Jönsson and Eklundh 2002) in order to compose a complete time

228   series. Pixels not flagged as "best quality", as determined from QA flags, were given a weight of zero

229   in the fitting algorithm to allow only pixels of best quality to be included. The width of the moving

230   window influences the degree of smoothing and the ability of the filter to cope with rapid changes

231   (parameters used in the TIMESAT preprocessing are shown in Table 1). The polynomial fitting was

232   iterated and adapted to the upper part of the curve by assigning weights to data points above and below

233   the result of the previous step (Jönsson and Eklundh 2004). SCD was extracted in TIMESAT for SCE,

234   and the seasonal snow cover integral (SCI) (defined as the integral under the curve between onset and

235   end of seasonal snow cover) was extracted to evaluate the accumulated seasonal SCE for each season.

236   Areas characterized by limited seasonal variability were masked out due to the inability of the

237   TIMESAT algorithm to estimate SCD for such conditions. The mask was created from the median of

238   the 16 seasons and excluded areas with less than 16 days in the SCD dataset. Most excluded areas were

239   located in glacier accumulation zones where constant snow cover prevents seasonal variability in SCE.

240

241   Table 1: Input parameters for use in TIMESAT.

Parameter	NDSI Snow Cover	Snow Albedo
Seasonal parameter	0.7	0.7
Number of envelope iterations	3	3
Adaptation strength	2	2
Savitzky-Golay window size	15	15
Spike Method	Median filter	Median filter
Amplitude season start (%)	70	65
Amplitude season end (%)	20	46

242

243   *4.2 Trend estimation*

244   We conducted linear temporal trend analysis to estimate the magnitude and direction of changes

245   in SCE, SAL, SCD, SCI, MAAT, and annual precipitation. We calculated per-pixel trends by applying

246   a nonparametric linear regression model with time as the independent variable and the abovementioned

247   variables as dependent variables. Since time series of the variables analyzed often do not meet

10

248   parametric assumptions of normality and homoscedasticity, a median trend (Theil–Sen, TS) procedure

249   was applied using the Theil-Sen slope estimator (median trend) which has proven robust against

250   outliers (Eastman 2009). Uncertainty estimates of trends are calculated from standard deviations of the

251   calculated metrics and are provided as ± values to all trends reported. The significance of the trends

252   was determined using the nonparametric Mann–Kendall test of significance (Mann 1945; Kendall

253   1975). The Mann–Kendall significance test is commonly used as a trend test for the TS median slope

254   operator (Eastman 2009) and produces outputs of z-scores that allow for the assessment of both the

255   significance and direction of trends. The trends were considered significant at $p < 0.05$ (where p

256   denotes the probability that there is no significant difference between observations over time). Trends

257   in SCE, SCD, and SCI were extracted from the area of maximum values (minimum of 75% at any

258   given time) for the entire study period and similar for SAL.

259

260   **5. Results**

261   *5.1 Spatio-temporal patterns in snow cover extent*

262   Statistical analysis of the MODIS time series revealed that the minimum, median, and

263   maximum SCE for the entire observation period and area (Fig. 2) was 2 %, 43 %, and 74 %,

264   respectively. SCE showed the presence of a clear linear relationship with elevation (coefficient of

265   determination (r^2) = 0.95, $p < 0.01$; Fig. 2d). However, the relationship was imperfect ($r^2 = 0.34$) above

266   4,000 m a.s.l due to increased scattering in the accumulation zone of the glaciers. At its maximum, SCE

267   covered 1,730 km^2 (74%) of the study area, only being present at elevations above 1,250 m a.s.l. SCE

268   area was normally distributed with highest consentration of SCE observed between 3,250 and 4,000 m

269   a.s.l. (Fig. 2e). SCE was on average ~11 % less on the eastern side of the Cordillera compared to the
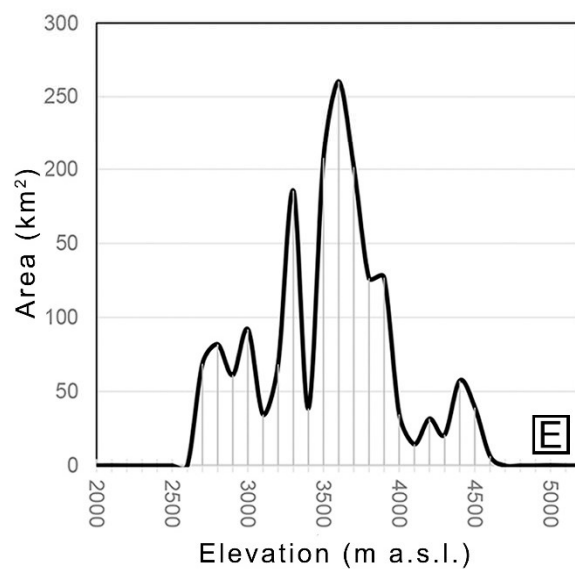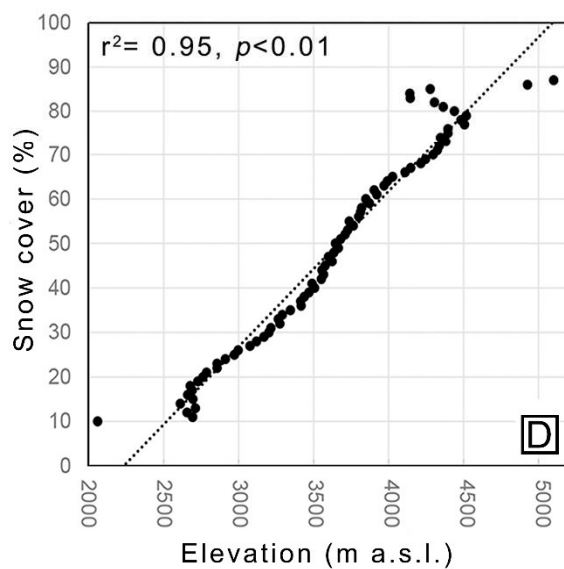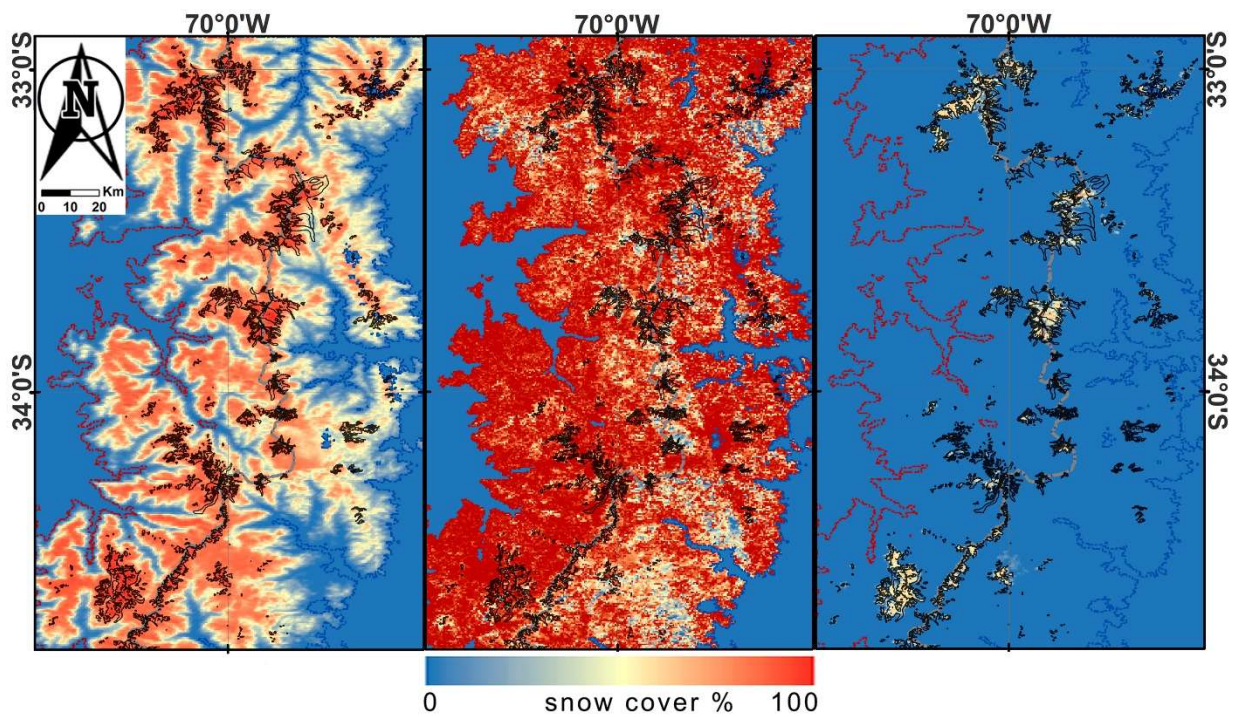
270   west (Fig. 2a-c).

271

Figure 2: a) Median snow extent; b) maximum snow cover extent; c) minimum snow cover extent for the 16 snow seasons observed (2000–2016) (glaciers are delineated by black); d) Mean SCE change with elevation; and e) Snow covered area distribution with elevation.

5.2 Inter- and intra-annual variability in snow cover extent (SCE) and snow albedo (SAL)

The mean SCE over the study area between 2000 and 2016 was approximately ~25 % in austral summer and ~68 % in austral winter, reaching a maximum between July 24th and 25th October and a minimum in autumn between March 6th and June 6th (Fig. 3). Overall, spatial trends for SCE and SAL showed widespread downward tendencies (Fig. 4). For SCE, downward trends dominated, with medium SCE decreasing by 13.4±4.0.x % between 2000 and 2016 (0.35 % yr^{-1}). Demonstrating spatial variabilities, the downward trends in SCE were found to be more pronounced for the the eastern side of the Cordillera (13.9±4.0 %, 0.9 % yr^{-1}) compared to the west (12.4±3.1 %, 0.8 % yr^{-1}). The eastern side of the Cordillera also showed lower SCE but higher SCE variability compared to the western side, this despite the eastern side being more elevated (mean elevation for the western and eastern sides is 3,115 m a.s.l and 3,720 m a.s.l, respectively) (Fig. 2d). Median SAL trends from March 2000 to Feburary 2016 were also downward with mean values decreasing by 7.4±2.2 % (0.5 % yr^{-1}). Downward trends in SAL were shown to be more widespread in the southern parts of the study area compared to northern parts. However, we found no significant differences between the eastern and western sides of the Cordillera.
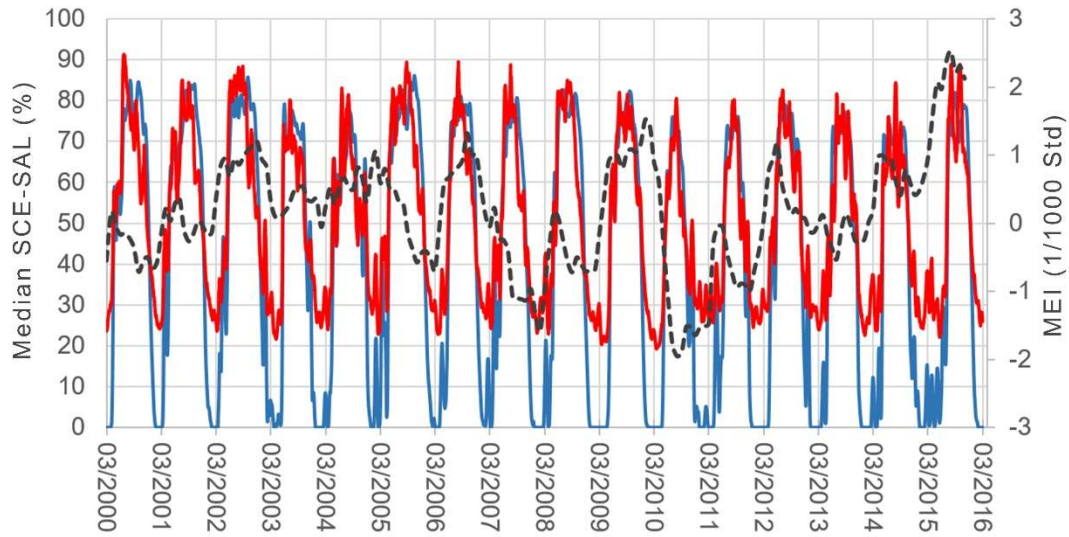
Figure 3: Variation in daily median SCE (blue) and median SAL (red) percentage and the bi-monthly multivariate ENSO index (MEI) (dark dashed line) in 1/1000 standard variations (Wolter and Timlin 2011).

13
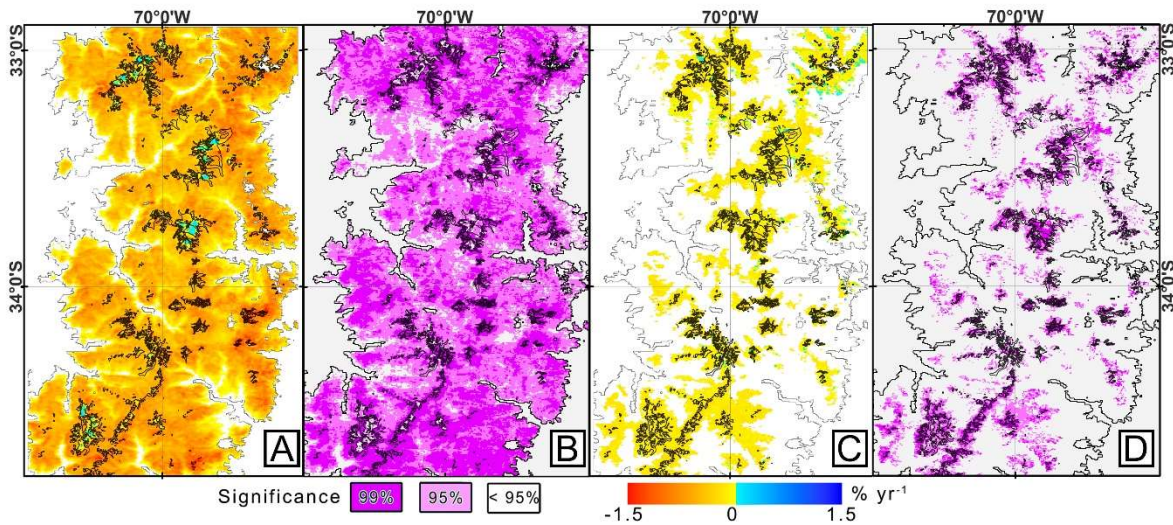
Figure 4: Linear median trend (*p*<0.05) in: SCE (a) and SAL (c) from Mar 2000 through Feb 2016, and the corresponding significance level of each trend (b, d).

Comparisons with SRTM data, the SAL trends observed showed negative correlations below ~4,600 m a.s.l. (-1.1 ± 0.8 % yr^{-1}, r=0.84, *p* < 0.01). Above ~4,600 m a.s.l., however, a distinct shift is observed, with increasing correlations as a function of elevation (0.2 ± 0.01 % yr^{-1}, r=0.83, *p* < 0.01) (Fig. 5). In regards to intra-annual variability, SCE showed pronounced downward trends (<-1 % yr^{-1}) during the onset (April, May, and June) and offset (October, November, December, and January) of the snowy season. In comparison to SCE, SAL showed slightly less intra-annual variability with most downward trends occurring during the onset of the snowy season (Fig. 6).

311
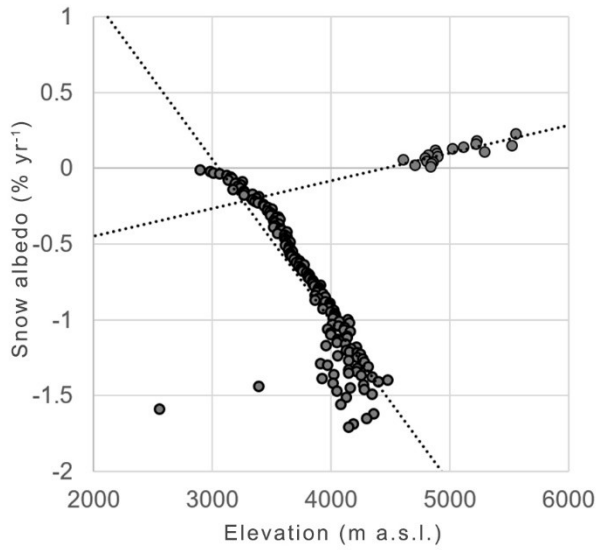
312 Figure 5: Trends in snow albedo (SAL) with elevation.

313

314

315
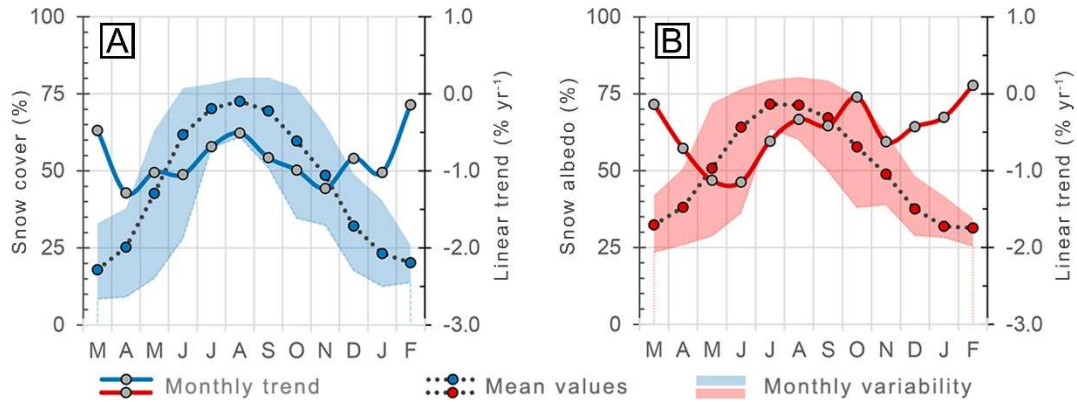
316 Figure 6: Intra-annual linear trends (blue and red lines), monthly mean values (dotted lines) and spread

317 (colored areas; monthly minimum and maximum values)) in: (a) snow cover extent (SCE); and (b)

318 snow albedo (SAL) between 2000 and 2016.

319

320 *5.3 Snow cover duration (SCD) and seasonal snow cover integral (SCI)*

321   The seasonal SCD values ranged between 0 and 280 days and the seasonal mean SCD ranged

322 between 203 days in the 2005–2006 to 130 days in 2011−2012, with an overall median of 173 days

323 (Fig. 7a). We observed a strong correlation between SCD and elevation (excluding glacier areas). SCD,

324 for example was shown to increase by an average of ~6 days for every 100-meter increment within the

15

2,000 to 4,600 m a.s.l. elevation range (r^2=0.80, p<0.01) (Fig. 7a). Overall, the trends in SCD were downward, showing a mean reduction of 43 ± 20 days for the study period (-2.7 ± 1.3 days yr^{-1}) (Fig. 8a). Trends were especially negative on the eastern side of the Cordillera, with a reduction of 52 ± 36 days (3.3 ± 2.3 days yr^{-1}), whereas on the western side SCD reduced by 35 ± 33 days (2.2 ± 2.0 days yr^{-1}).
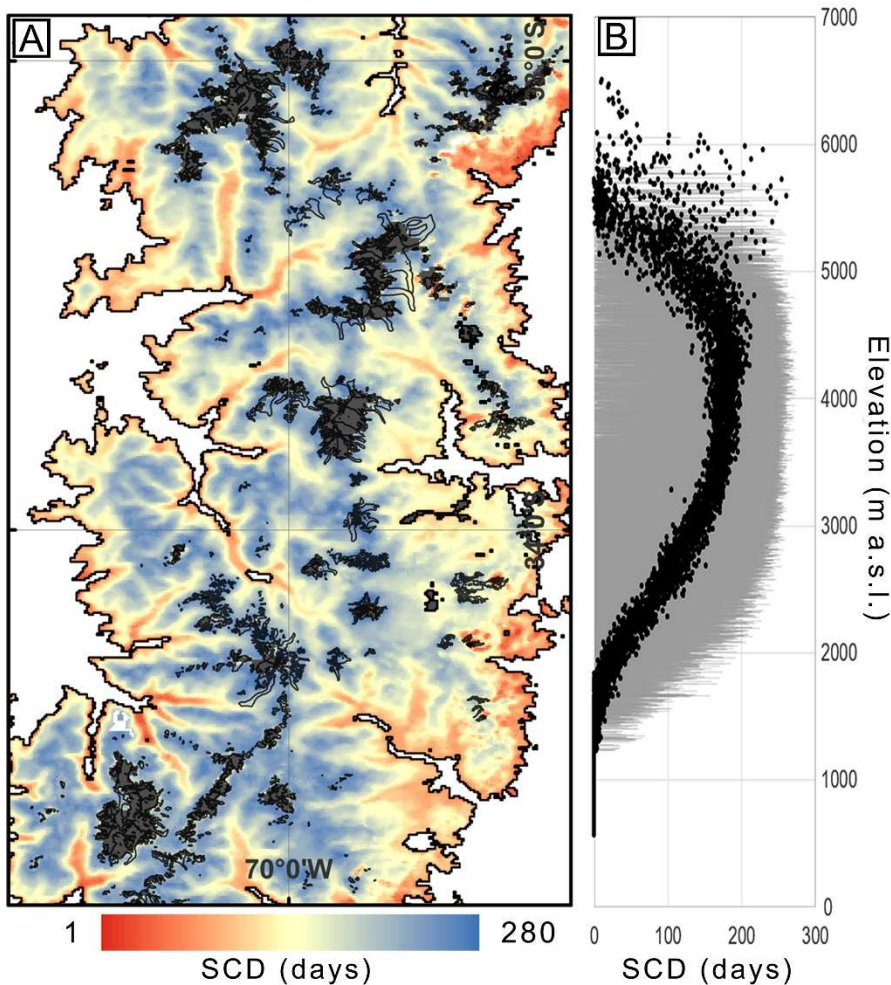
Figure 7: a) Median snow cover duration (SCD, days) 2000−2016 (dark grey areas represent locations where the model failed to determine seasonality); and (b) Mean snow cover duration with elevation for the 2000−2016 period (grey bars show the spread between minimum and maximum values of SCD as a function of elevation).

337

Figure 8: (a) Per pixel yearly snow cover duration (SCD) trend 2000–2016, and (b) corresponding

significance of trend. Dark gray masked areas represent the mask where SCD values are erroneous and

black lines represent glaciers.

341

The SCI for the entire study area declined by 1.5 ± 0.5 % yr^{-1} (median trend), corresponding to 25 ± 8

% during the full period of 16 snow seasons. The SCI also shows substantial inter-annual variation

(Fig. 9), especially on the eastern side of the Cordillera, where SCI is on average 17 % smaller and

trends are substantially more downward (1.8 ± 0.5 % yr^{-1}) than for the western side (1.2 ± 0.4 % yr^{-1}).

346
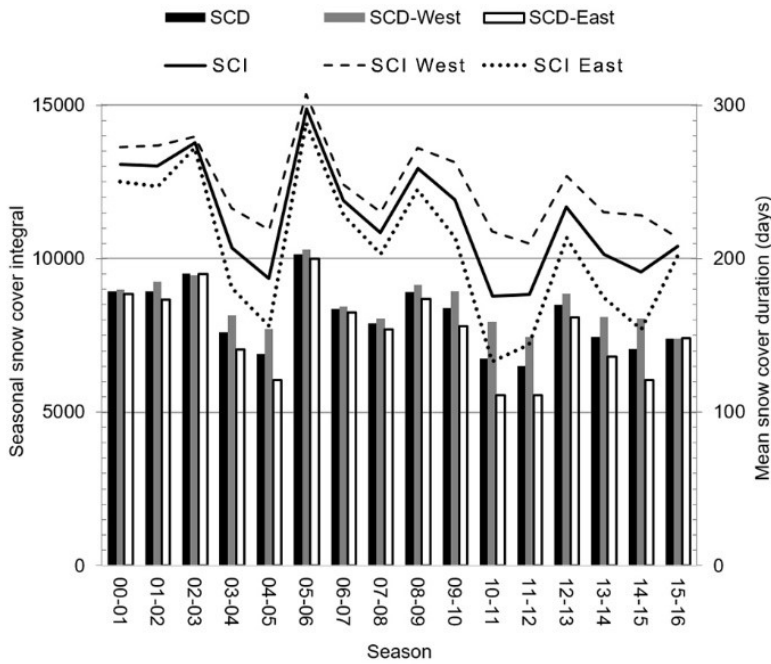
Figure 9: Mean snow cover duration (SCD, bars) and seasonal snow cover integral (SCI, lines) for the

entire study area and for the western (SCD-W) and eastern (SCD-E) sides of the cordillera separately.

350

5.4 Impact of changes in temperature, precipitation, and El Niño Southern Oscillation (ENSO) on snow

cover duration and snow albedo

Analysis of the meteorological data available from the EYE weather station (Figure 1b)

revealed a significant downward trend in precipitation of -4 mm yr^{-1} and an insignificant trend in

355 MAAT of 0.05°C yr⁻¹ between 2000 and 2016. Between 2000 and 2009, nine extreme precipitation

356 events (>200 mm month⁻¹) were identified, with the 2003-2004 season (March-February) receiving a

357 maximum of 1,259 mm. These 'extreme' events occurred mostly during austral winters and account for

358 large differences in inter-annual precipitation amounts, SCE and SCD sums. Post 2009, no extreme

359 precipitation events occurred, however a minimum of 317 mm was observed for the 2014-2015 season.

360 The mean annual precipitation sum for the 2000 to 2016 observation period was 677 mm. MAAT for

361 this observation period was 9.0°C, with maximum and minimum values of 10.3°C and 7.3°C measured

362 for the 2003-2004 and 2011-2012 seasons, respectively.

363   Statistical comparisons between the MODIS-derived snow data and the observed EYE

364 meteorological data revealed that monthly SCE and SAL averaged over the study area correlated

365 strongly with MMAT (r^2-values of 0.74 and 0.84, respectively) (Fig. 10a-b). Mean monthly SCE and

366 SAL also correlate with monthly precipitation sums, but to a lesser extent (r^2-values of 0.20 and 0.28)

367 (Fig. 10c-d). In comparison, SCI correlated more strongly with annual precipitation sums (r^2-value of

368 0.84) (Fig. 10e).

369
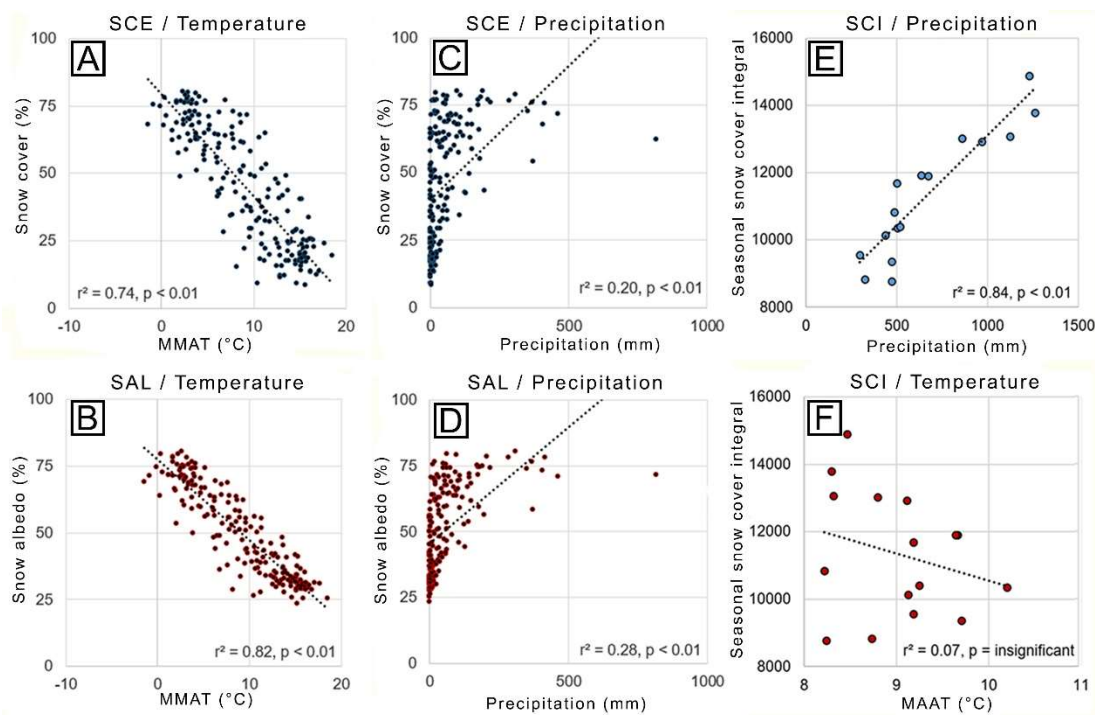
371 Figure 10: Relationships between monthly meteorological data (EYE station; Fig. 1) and monthly SCE,

372 monthly SAL, and SCI averaged over the study area. a) Monthly SCE against MMAT; b) monthly SAL

against MMAT, c) Monthly SCE against monthly precipitation sums, d) Monthly SCE against monthly

precipitation sums, e) SCI against annual precipitation sums, and f) SCI against MAAT.

ENSO events (MEI) (plotted in Fig. 3) show significant correlations with mean SCE and SAL

values for the study area (Fig. 11). Mean correlation coefficient values (r) between MEI and SCE/SAL

were strongest when a lag of one month (L1) was applied to the SCE/SAL time series (mean r-values

of 0.21 for the study area).

Generally, glaciated areas where snow cover is already present are characterized by negative

SCE and ENSO correlations for shorter lag periods (L1), which is in contrast to the surrounding snow

covered areas. This pattern is reversed for longer lag periods (e.g., five months), when glaciated and

higher elevated areas significantly correlate with ENSO, whereas surrounding lower altitude areas are

characterized by negative correlations.
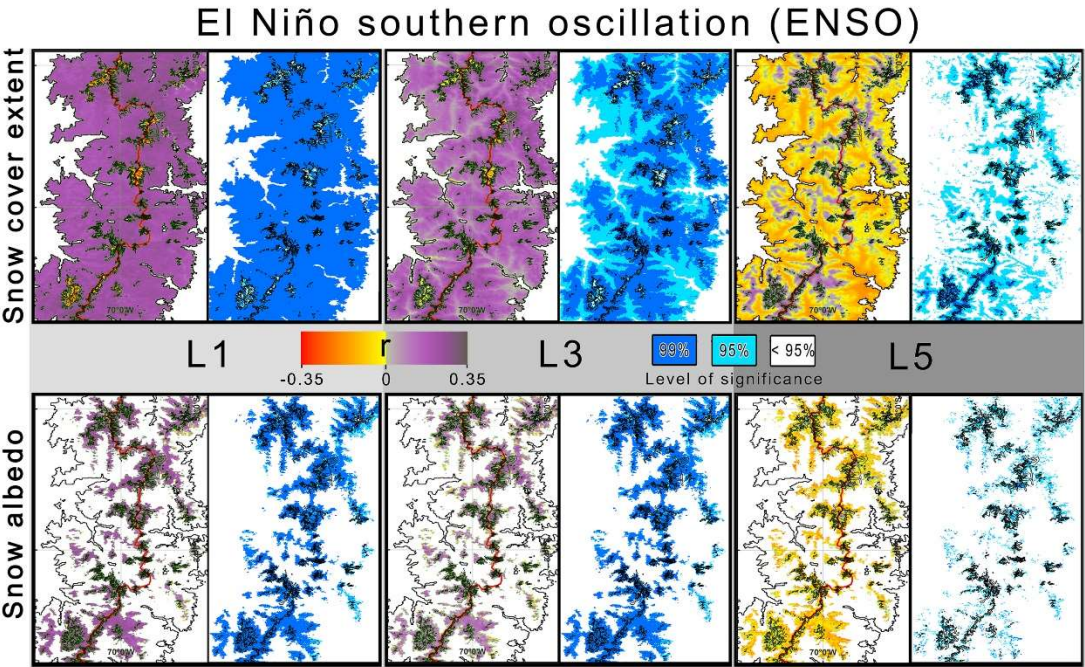
Figure 11: Per-pixel correlations and significance of SCE/SAL with the ENSO index (MEI) including

one-, three- and five-month lag time (L1, L3, and L5). Red line demarks the east west divide.

6. Discussion

391

6.1 Monitoring and assessment of snow cover and snow albedo

Spatio-temporal analysis of MODIS-derived SCE, SAL, SCD, and SCI data revealed significant changes during the observation period of this study. Key to the interpretation of these results is the quantification of sensor related errors and their influence on the trends observed (2000–2016). Unfortunately, only a few validation studies of the MOD10A1 C6 products have been published to date. Recent studies using MOD10A1 collection C6 for the Greenland ice sheet however found that v.C6 corrects for the C5 temporal trend bias in dry snow areas and that albedo retrieval accuracy in C6 is substantially improved over C5 (Box et al. 2017; Casey et al. 2017). Therefore, the accuracy of this product is expected to be better than or at least as good as the C5 product, which has been evaluated in several previous studies (Tekeli et al. 2005; Hall and Riggs 2007; Gao et al. 2010; Arsenault et al. 2014; Marchane et al. 2015). These studies estimate an overall detection error ranging from ~5 % to ~48 %, depending on locational properties and type of 'ground truth' observations used. In general, spatially homogeneous locations with flat terrain produces less error than in complex terrain with mixed surface as being the case for this study (Wang et al. 2014; Burakowski et al. 2015; Moustafa et al. 2017). By applying a per-pixel temporal change analysis approach in the current study, thereby avoiding direct inter-comparison of pixels characterized by different slope/aspect, the influence of topography is expected to be reduced to some degree. This should also be seen in the context of the latitudinal location of the study area (32°50'− 34°5050' S), characterized by an annual range in solar zenith angles of 28-60 for MODIS overpass times. This makes the region less prone to influences from mountain shadowing as compared to complex terrain of higher latitudes of the northern/southern hemisphere. Snow detection in v.6 is expected to show improvements in comparison to previous versions especially above 1.300 m a.s.l., where the surface temperature screen used in the product algorithm (which has previously caused false negatives) has been rolled back leaving fewer gaps in the data (Hall and Riggs 2016).

The smoothed and gap-filled MOD10A1 C6 dataset produced with TIMESAT is assumed to correctly represent the seasonal snow distribution for the area. Here, only the best quality MOD10A1 C6 observations (by including information available from the QA flags; 0="best quality") were used for the Savitzky-Golay function fitting in TIMESAT. By adjusting the data fitting to the upper envelope of the daily observations, we ensured that the SCE and SAL values follow rapid changes,

421 which can occur in snow cover extent and albedo. The TIMESAT model uses local function fitting,

422 where values before and after in the time series are considered. This local function fitting reduces the

423 chance of error occurrence in the MOD10A1 observed snow cover (Tekeli et al. 2005). For the upper

424 ablation zones of glaciers, characterized by limited seasonal variability or year round snow SCE, it is

425 not possible to accurately assess seasonality variables and thereby SCD. In this case, a glacier mask

426 was applied based on SCE seasonal variability, in doing so, restricting the SCD analysis to non-

427 glaciated areas (Fig. 7a). Out of all the pixels in the data series 24.2 % was filled with modeled data

428 from TIMESAT.

429   Snow albedo detection in mountainous environments from remotely sensed imagery can contain

430 large errors when measured on terrain with steep slopes. Validation of satellite or aerial imagery based

431 data using stationary point albedometers can also be challenging because of pronounced mixed pixel

432 and geolocation issues (Liang et al. 2005; Sorman et al. 2007; Mernild et al. 2015b; Box et al. 2017).

433 However, these issues are not likely to have significantly influenced the trends observed in this study as

434 the MOD10A1 pixels are measured in the same pixel location from year to year in a location where

435 seasonal variation in solar zenith angle influence is relatively low (annual range between 28-60

436 degrees) compared to higher latitudes of the northern/southern hemisphere. MOD10A1 snow albedo is

437 produced only for cloud free pixels with full snow cover (+50 %) indicating that for pixels

438 characterized by limited full snow cover observations seasonal fitting could have influenced the

439 accuracy of the TIMESAT generated data.

440

441 *6.2 Analysis of climate variables*

442   The analysis of the effect of local scale climatic variability presented in this study made use of

443 the only existing weather station EYE in the study area. Indeed, the use of a single station is not ideal

444 when comparing measurements with the spatially large-scale MOD10A1 dataset. Furthermore, given

445 the location of this weather station on the western side of the cordillera and the presence of distinct

446 climatic gradients (e.g. Mernild et al. 2016a), the data recorded is unlikely to be fully representative of

447 the study area as a whole. However, this scarce coverage of ground observations reflects the general

448 conditions for mountainous areas of the Andes and underlines the need for remotely sensed monitoring

449 methods.

450   Upward trends in MAAT have higher impact the lower the altitudes (mostly noticeable in the
451   southern part of the study area) causing changes in onset and offset of snow seasons to be more
452   sensitive to even small changes in temperature (Fig. 4). Low areas with small slope gradient show
453   higher sensitivity to upward changes in MAAT in regards to snow accumulation. Especially the low
454   elevated areas on the eastern side of the cordillera show the effect of increased MAAT.

455   Above 4,600 m a.s.l., SCD shows a considerable increase in variability (Fig. 7b). This however
456   is not surprising as, in highly elevated zones where SCD can be dependent on localized terrain (slope
457   and area of topographical shadow) and weather conditions. High wind speeds, for example, often make
458   it less likely for snow cover to persist in certain areas despite high levels of solid precipitation.

459

460   *6.3 Drivers of change on snow cover variables*

461   Studies based on modeling, field measurements and remote sensing have provided insights into
462   the past, current, and future impacts of climate change on snow conditions and runoff in the Andean
463   river catchments of central Chile and Argentina (Pelliccriotti et al. 2007; Apaloo et al. 2012; Delbart et
464   al. 2015; Mernild et al. 2015a, 2016a, 2016c; Ragettli et al. 2016). A number of these studies have
465   predicted that air temperatures in the central Andes will continue to increase. An increase in air
466   temperature, together with seasonal changes in precipitation patterns, will likely result in a decrease in
467   the amount of runoff from snow melt and an increase in the amount of runoff from rain (Cai et al.
468   2014; Mernild et al. 2016a, 2016c; Ragettli et al. 2016). Since the 1970's, precipitation events have
469   generally become more intense but less frequent in central Chile (Falvey and Garreaud 2007; Garreaud
470   et al. 2009). The EYE precipitation data, for example, shows a number of intense precipitation events
471   (above 200 mm m^{-1}) during the 2000–2009 period. Interestingly, none of these 'intense' events
472   occurred during the 2010–2016 period.

473   Per-pixel correlations between SCE/SAL and the Multivariate El Niño index (MEI) show that
474   MEI has a strong and significant impact on inter-annual SCE/SAL variability in the region (Fig. 11).
475   Although El Niño events are often associated with increases in precipitation, they can also be
476   associated with increases in air temperature (Cai et al. 2014) which, together, can have a pronounced
477   altitude dependent effect on snow cover during spring and autumn. An increase in air temperature, for
478   example, causes the 0°C isotherm to ascend to higher elevations resulting in a larger proportion of
479   precipitation falling as rain as opposed to snow. Mernild et al. (2016c) observed this phenomenon for

22

480 the Olivares basin (33°12' S; 70°09' W) between 1979 and 2014, where precipitation has been

481 increasingly falling as rain in recent years. This change in the partitioning of precipitation over

482 mountainous areas can offset the positive effects of increased precipitation on snow accumulation, with

483 rainfall often enhancing snow and ice melt rates on glacier surfaces. The significant spatial variation in

484 correlation between MEI and SCE for one-month lag, we suspect is caused by the presence of snow

485 cover on glaciers giving negative or no correlation on short term but increasing correlations with time.

486   Reduction in SCE in this study has also been studied in modelling studies based on MERRA

487 satellite data (Mernild et al. 2016b, 2016c) which estimate that snow cover extent in the central Andes

488 has reduced ~1.3% per decade 2000–2014 (linear trend, for the b1 window in Fig. 1) (Mernild et al.

489 2016b). Mernild et al. (2016c) suggest that the largest decreases in snow cover have occurred within

490 the 3,000–5,000 m a.s.l. elevation range, where more than 70 % of seasonal precipitation falls as snow.

491 In comparison, the rate of SCE change observed in this study for the same period and area is

492 significantly higher, with per decade reductions equating to ~2.8%. This difference between the results

493 presented here and in Mernild et al. (2016c) may either be an indicator of faster SCE reduction during

494 the 2000–2016 period or highlight possible SCE overestimations in the MERRA model utilized by the

495 latter. For other regions of the world snow cover reductions are well documented. In the Arctic, for

496 example, a general decease in the amount of snow has been observed between 1999 and 2009, together

497 with reductions in maximum winter snow water equivalent, a later snow-cover onset in autumn and

498 earlier snow-free date in spring, and a decreasing snow-cover duration (Liston and Hiemstra 2011).

499 To sustain all year runoff, rivers of the central Andes rely on substantial contributions from snow and

500 ice-melt, and river discharge here is strongly linked to snow cover changes (Delbart et al. 2015).

501 Decreases in SCE at the magnitudes shown in this study has the potential to cause a substantial

502 redistribution in seasonal runoff for this region, where ~21 % of river runoff originates from snow- and

503 ice- melt (increasing to ~85 % during dry summers) (Peña and Nazarala 1987; Mernild et al. 2016a).

504 Glaciers in the central Andes are shrinking and down wasting as a consequence of climate warming and

505 changes in precipitation patterns (Masiokas et al. 2006; Bodin et al. 2010; Gacitua et al. 2015; Malmros

506 et al. 2016). Although initially increasing, ice melt runoff will begin to reduce in the future as lowest

507 elevation land ice disappears. If these ice/snow cover trends continue, runoff conditions will likely

508 change, especially during spring, dry summers and periods of drought, affecting the future

509 sustainability of freshwater resources in areas downstream of the central Andes (Peña and Nazarala

510   1987; Delbart et al. 2015; Saavedra et al. 2016; Carey et al. 2017; López-Moreno et al. 2017). Whether

511   this change in runoff will cause the low lying areas in the catchment to become wetter or drier is

512   largely determined by local topography (Polk et al. 2017, López-Moreno et al. 2017).

513   Directly influencing the surface energy balance, the downward trends in SAL revealed in this

514   study (Fig. 4) may possibly result in positive feedbacks in regards to snow and ice melt. This trend of

515   darkening surfaces, either from reduced snow cover or from enhanced melt conditions, is likely to be

516   reinforced by increasing air temperatures and decreasing precipitation (e.g., Mernild et al. 2016c).

517   Another positive feedback could be initiated by the accumulation of dust and debris on glacier surfaces

518   leading to more energy being absorbed and further melt conditions, especially on lower parts of

519   glaciers (Hansen and Nazarenko 2004; Oerlemans et al. 2009; Arenson et al. 2015). Minimum glacier-

520   wide albedo has shown to be a good predictor for glacier mass balances conditions for temperate

521   glaciers (López-Moreno et al. 2017; Polk et al. 2017), which suggests that glaciers in the study area

522   may have positive mass balances, at least for some of the years analyzed. Decreases in surface albedo

523   have also been observed for many other glaciated parts of the world (Box et al. 2012; Tedesco et al.

524   2013; Abermann et al. 2014; Fausto et al. 2015; Mernild et al. 2015b). The mean albedo for the

525   Greenland ice sheet ablation area (June–August), for example, declined by 22.9 % from 2000 to 2016

526   while dry snow areas only decreased by 1.2 % (Box et al. 2017). Increasing albedo values seen above

527   4.600 m a.s.l. (Fig. 5.) are likely contributed to by the increase in precipitation and the presence of dry

528   snow conditions at high altitudes (Box et al. 2017).

529   The central Andes are dominated by two distinctly different climate systems. On the western

530   side of the Cordillera the climate is influenced by oceanic atmospheric interactions, whereas on the

531   eastern side the climate can be considered continental in type (Prohaska 1976). This difference in

532   climate is highlighted in this study by the relatively weak correlation between SCE/SAL and MEI on

533   the eastern side of the Cordillera compared to the west. A higher inter-annual variability in SCE and

534   SCI and more downward trend on the eastern part may be contributed to continental climate conditions

535   (Fig. 9) as also observed in Saavedra et al. 2017.

536

537   **7. Conclusions and outlook**

538   Overall, snow cover extent (SCE) and snow albedo (SAL) decreased by 13.4 ± 4 % and 7.4 ± 2

539   %, respectively, between 2000 and 2016. SCE showed more downward trends on the eastern side of the

Andes Cordillera (13.9 ± 4 %), while SAL showed a uniform decline thrughout the area. A seasonal analysis revealed downward trends in SCE and SAL for all months of the year, with the largest decreases occuring during the onset (for SCE and SAL) and at the end of the snow seasons (for SCE) (> 1% yr^{-1}). SCE showed a near linear increase with elevation (r^2=0.96, $p < 0.01$), and largest relative losses occuring at elevations above 4.600 m a.s.l. outside glaciated areas. Spatial anaysis of the SAL data revealed increasingly downward trends up to ~4,600 m a.s.l. in elevation. Above ~4,600 m a.s.l. this trend is reversed, likely because of permanent or semi-permanent dry snow conditions present in glacier accumulation zone. Snow cover duration (SCD) decreased on average by 43 ± 20 days throughout the study area between 2000 and 2016 with largest changes occuring at elevations below 4.500 m a.s.l. on the eastern side and 3.500 m a.s.l. on the western side.

TIMESAT was unable to extract SCD for glacier areas that were covered with snow for most of the year due to the lack of seasonal variation. Additionally, in situations of large variations in snow conditions occuring over a very short time period the Savitzky-Golay seasonal fitting process applied may introduce some errors. SCD trends for the study area indicate a shortening of the snow season between 2000 and 2016. SCI trends for the included glacial areas were also shown to be downward during this 16-year observation period (these being more pronounced on the eastern side of the Cordillera).

The impact of ENSO events, which influence largescale precipitation and temperature patterns in the study area, on the SCE, SCD, and SAL was shown to be evident. Per-pixel analyses revealed that ENSO positively influences SCE/SAL values most strongly with a one-month time-lag. Data available from the EYE meteorological station, between 2000 and 2016, reveals that the monthly SCE and SAL values are primarliy determined by variations in temperature, whilst montly SCI values are determined mostly by precipitation. If the observed decline in SCE persist in the coming years, it will likely result in a a seasonal redistribution of avaliable downstream freshwater which may cause future problems for people and agriculture in the region.

Acknowledgements

569   #1140172. All data requests should be addressed to the first author. The authors have no conflict of

570   interest.

571

572

573   **References:**

574   Abermann, J., Kinnard, C., & MacDonell, S. (2014). Albedo variations and the impact of clouds on

575   glaciers in the Chilean semi-arid Andes. *Journal of Glaciology, 60*, 183-191

576   Apaloo, J., Brenning, A., & Bodin, X. (2012). Interactions between Seasonal Snow Cover, Ground

577   Surface Temperature and Topography (Andes of Santiago, Chile, 33.5°S). *Permafrost and*

578   *Periglacial Processes, 23*, 277-291

579   Arenson, L.U., Jakob, M., & Wainstein, P. (2015). Effects of Dust Deposition on Glacier Ablation and

580   Runoff at the Pascua-Lama Mining Project, Chile and Argentina. In G. Lollino, A. Manconi, J.

581   Clague, W. Shan, & M. Chiarle (Eds.), *Engineering Geology for Society and Territory - Volume*

582   *1: Climate Change and Engineering Geology* (pp. 27-32). Cham: Springer International

583   Publishing

584   Arsenault, K.R., Houser, P.R., & De Lannoy, G.J.M. (2014). Evaluation of the MODIS snow cover

585   fraction product. *Hydrological Processes, 28*, 980-998

586   Benn, D.I., & Evans , D.J.A. (2010). *Glaciers and glaciation*. London: Hodder Education

587   Bodin, X., Rojas, F., & Brenning, A. (2010). Status and evolution of the cryosphere in the Andes of

588   Santiago (Chile, 33.5 degrees S.). *Geomorphology, 118*, 453-464

589   Box, J.E., Fettweis, X., Stroeve, J.C., Tedesco, M., Hall, D.K., & Steffen, K. (2012). Greenland ice

590   sheet albedo feedback: thermodynamics and atmospheric drivers. *The Cryosphere, 6*, 821-839

591   Box, J.E., Van As, D., Steffen, K., Fausto, R.S., Ahlstrøm, A.P., Citterio, M., & Andersen, S.B. (2017).

592   Greenland, Canadian and Icelandic land-ice albedo grids (2000–2016). *Geol. Surv. Den.*

593   *Greenl. Bull, 38,* 53-56

594   Brock, B.W., Willis, I.C., & Sharp, M.J. (2000). Measurement and parameterization of albedo

595   variations at Haut Glacier d'Arolla, Switzerland. *Journal of Glaciology, 46*, 675-688

596   Burakowski, E.A., Ollinger, S.V., Lepine, L., Schaaf, C.B., Wang, Z., Dibb, J.E., Hollinger, D.Y., Kim,

597   J., Erb, A., & Martin, M. (2015). Spatial scaling of reflectance and surface albedo over a mixed-

use, temperate forest landscape during snow-covered periods. Remote Sensing of Environment, 158, 465-477

Cai, W., Borlace, S., Lengaigne, M., van Rensch, P., Collins, M., Vecchi, G., Timmermann, A., Santoso, A., McPhaden, M.J., Wu, L., England, M.H., Wang, G., Guilyardi, E., & Jin, F.-F. (2014). Increasing frequency of extreme El Nino events due to greenhouse warming. *Nature Clim. Change, 4*, 111-116

Carey, M., Molden, O.C., Rasmussen, M.B., Jackson, M., Nolin, A.W., & Mark, B.G. (2017). Impacts of Glacier Recession and Declining Meltwater on Mountain Societies. *Annals of the American Association of Geographers, 107*, 350-359

Casey, K.A., Polashenski, C.M., Chen, J., & Tedesco, M. (2017). Impact of MODIS sensor calibration updates on Greenland Ice Sheet surface reflectance and albedo trends. *The Cryosphere, 11,* 1781-1795Cereceda-Balic, F., Palomo-Marín, M.R., Bernalte, E., Vidal, V., Christie, J., Fadic, X., Guevara, J.L., Miro, C., & Pinilla Gil, E. (2012). Impact of Santiago de Chile urban atmospheric pollution on anthropogenic trace elements enrichment in snow precipitation at Cerro Colorado, Central Andes. *Atmospheric Environment, 47*, 51-57

Cornwell, E., Molotch, N.P., & McPhee, J. (2016). Spatio-temporal variability of snow water equivalent in the extra-tropical Andes Cordillera from distributed energy balance modeling and remotely sensed snow cover. *Hydrology and Earth System Sciences, 20*, 411-430

Corripio, J.G., & Purves, R.S. (2006). Surface Energy Balance of High Altitude Glaciers in the Central Andes: The Effect of Snow Penitentes. *Climate and Hydrology in Mountain Areas* (pp. 15-27): John Wiley & Sons, Ltd

Cuffey, K.M., & Paterson, W.S.B. (2010). *The Physics of Glaciers*. Elsevier Science

Dariane, A.B., Khoramian, A. & Santi, E. (2017). Investigating spatiotemporal snow cover variability via cloud-free MODIS snow cover product in Central Alborz Region. *Remote Sensing of Environment, 202,* 152-165.

Delbart, N., Dunesme, S., Lavie, E., Madelin, M., & Goma, R. (2015). Remote sensing of Andean mountain snow cover to forecast water discharge of Cuyo rivers. *Journal of Alpine Research*, 15

Dozier, J., & Frew, J. (1981). Atmospheric Corrections to Satellite Radiometric Data over Rugged Terrain. *Remote Sensing of Environment, 11*, 191-205

628   Dozier, J., Painter, T.H., Rittger, K., & Frew, J.E. (2008). Time-space continuity of daily maps of
629   fractional snow cover and albedo from MODIS. *Advances in Water Resources, 31*, 1515-1526

630   Dubayah, R. (1992). Estimating Net Solar-Radiation Using Landsat Thematic Mapper and Digital
631   Elevation Data. *Water Resources Research, 28*, 2469-2484

632   Dumont, M., Gardelle, J., Sirguey, P., Guillot, A., Six, D., Rabatel, A., & Arnaud, Y. (2012). Linking
633   glacier annual mass balance and glacier albedo retrieved from MODIS data. *The Cryosphere, 6*,
634   1527-1539

635   Eastman, J.R. (2009). IDRISI Taiga guide to GIS and image processing. *Clark Labs Clark University,*
636   *Worcester, MA*

637   Eklundh, L., & Jönsson, P. (2015). TIMESAT: A Software Package for Time-Series Processing and
638   Assessment of Vegetation Dynamics. In C. Kuenzer, S. Dech, & W. Wagner (Eds.), *Remote*
639   *Sensing Time Series: Revealing Land Surface Dynamics* (pp. 141-158). Cham: Springer
640   International Publishing

641   Escobar, F., Casassa, G., & Pozo, V. (1995). Variaciones de un glaciar de Montaña en los Andes de
642   Chile Central en las últimas dos décadas. *Bulletin de l'Institut français d'études andines, 24*,
643   683-995

644   Falvey, M., & Garreaud, R. (2007). Wintertime Precipitation Episodes in Central Chile: Associated
645   Meteorological Conditions and Orographic Influences. *Journal of Hydrometeorology, 8*, 171-
646   193

647   Falvey, M., & Garreaud, R.D. (2009). Regional cooling in a warming world: Recent temperature trends
648   in the southeast Pacific and along the west coast of subtropical South America (1979-2006).
649   *Journal of Geophysical Research-Atmospheres, 114*

650   Farr, T.G., Rosen, P.A., Caro, E., Crippen, R., Duren, R., Hensley, S., Kobrick, M., Paller, M.,
651   Rodriguez, E., Roth, L., Seal, D., Shaffer, S., Shimada, J., Umland, J., Werner, M., Oskin, M.,
652   Burbank, D., & Alsdorf, D. (2007). The Shuttle Radar Topography Mission. *Reviews of*
653   *Geophysics, 45*, n/a-n/a

654   Fausto, R.S., van As, D., Antoft, J.A., Box, J.E., Colgan, W., & Team, P.P. (2015). Greenland ice sheet
655   melt area from MODIS (2000-2014). *Geological Survey of Denmark and Greenland Bulletin*,
656   57-60

657 Gacitua, G., Uribe, J.A., R., W., Loriaux, T., Hernandez, J., & Rivera, A. (2015). 50MHz helicopter-
658   borne radar data for determination of glacier thermal regime in the central Chilean Andes.
659   *Annals of Glaciology, 56*

660 Gao, Y., Xie, H.J., Yao, T.D., & Xue, C.S. (2010). Integrated assessment on multi-temporal and multi-
661   sensor combinations for reducing cloud obscuration of MODIS snow cover products of the
662   Pacific Northwest USA. *Remote Sensing of Environment, 114*, 1662-1675

663 Gardner, A.S., & Sharp, M.J. (2010). A review of snow and ice albedo and the development of a new
664   physically based broadband albedo parameterization. *Journal of Geophysical Research-Earth*
665   *Surface, 115*

666 Garreaud, R.D., Vuille, M., Compagnucci, R., & Marengo, J. (2009). Present-day South American
667   climate. *Palaeogeography Palaeoclimatology Palaeoecology, 281*, 180-195

668 Gurung, D. R., Maharjan, S. B., Shrestha, A. B., Shrestha, M. S., Bajracharya, S. R. and Murthy, M. S.
669   R. (2017). Climate and topographic controls on snow cover dynamics in the Hindu Kush
670   Himalaya. *Int. J. Climatol., 37*: 3873–3882.

671 Hall, D.H., & Riggs, G. (2016). MODIS/Terra Snow Cover Daily L3 Global 500m Grid, Version 6. In
672   National Snow and Ice Data Center (NSIDC) (Ed.). Boulder, Colorado USA: NASA

673 Hall, D.K., & Riggs, G.A. (2007). Accuracy assessment of the MODIS snow products. *Hydrological*
674   *Processes, 21*, 1534-1547

675 Hall, D.K., Riggs, G.A., & Salomonson, V.V. (1995). Development of methods for mapping global
676   snow cover using moderate resolution imaging spectroradiometer data. *Remote Sensing of*
677   *Environment, 54*, 127-140

678 Hall, D.K., Riggs, G.A., Salomonson, V.V., DiGirolamo, N.E., & Bayr, K.J. (2002). MODIS snow-
679   cover products. *Remote Sensing of Environment, 83*, 181-194

680 Hansen, J., & Nazarenko, L. (2004). Soot climate forcing via snow and ice albedos. *Proceedings of the*
681   *National Academy of Sciences of the United States of America, 101*, 423-428

682 Hock, R. (2005). Glacier melt: a review of processes and their modelling. *Progress in Physical*
683   *Geography, 29*, 362-391

684 Huang, X., Deng, J., Wang, W., Feng, Q. & Liang, T. (2017). Impact of climate and elevation on snow
685   cover using integrated remote sensing snow products in Tibetan Plateau. *Remote Sensing of*
686   *Environment, 190,* 274-288.

687   Jönsson, P., & Eklundh, L. (2002). Seasonality extraction by function fitting to time-series of satellite

688   sensor data. *Ieee Transactions on Geoscience and Remote Sensing, 40*, 1824-1832

689   Jönsson, P., & Eklundh, L. (2004). TIMESAT - a program for analyzing time-series of satellite sensor

690   data. *Computers & Geosciences, 30*, 833-845

691   Justice, C.O., Vermote, E., Townshend, J.R.G., Defries, R., Roy, D.P., Hall, D.K., Salomonson, V.V.,

692   Privette, J.L., Riggs, G., Strahler, A., Lucht, W., Myneni, R.B., Knyazikhin, Y., Running, S.W.,

693   Nemani, R.R., Wan, Z.M., Huete, A.R., van Leeuwen, W., Wolfe, R.E., Giglio, L., Muller, J.P.,

694   Lewis, P., & Barnsley, M.J. (1998). The Moderate Resolution Imaging Spectroradiometer

695   (MODIS): Land remote sensing for global change research. *Ieee Transactions on Geoscience*

696   *and Remote Sensing, 36*, 1228-1249

697   Kendall, M.G. (1975). *Rank Correlation Methods*. London: Griffin

698   Klein, A.G., & Stroeve, J. (2002a). Development and validation of a snow albedo algorithm for the

699   MODIS instrument. *Annals of Glaciology, Vol 34, 2002, 34*, 45-52

700   Klein, A.G., & Stroeve, J. (2002b). Development and validation of a snow albedo algorithm for the

701   MODIS instrument. *Annals of Glaciology, 34*, 45-52

702   Knap, W.H., Brock, B.W., Oerlemans, J., & Willis, I.C. (1999). Comparison of Landsat TM-derived

703   and ground-based albedos of Haut Glacier d'Arolla, Switzerland. *International Journal of*

704   *Remote Sensing, 20*, 3293-3310

705   Konzelmann, T., & Ohmura, A. (1995). Radiative Fluxes and Their Impact on the Energy-Balance of

706   the Greenland Ice-Sheet. *Journal of Glaciology, 41*, 490-502

707   Leiva, J.C. (1999). Recent fluctuations of the Argentinian glaciers. *Global and Planetary Change, 22*,

708   169-177

709   Li, C., Su, F., Yang, D., Tong, K., Meng, F. and Kan, B. (2017). Spatiotemporal variation of snow

710   cover over the Tibetan Plateau based on MODIS snow product, 2001–2014. *Int. J. Climatol.*

711   doi:10.1002/joc.5204

712   Li, X., Fu, W., Shen, H., Huang, C. & Zhang, L. (2017). Monitoring snow cover variability (2000–

713   2014) in the Hengduan Mountains based on cloud-removed MODIS products with an adaptive

714   spatio-temporal weighted method. *Journal of Hydrology, 551,* 314-327.

715   Liang, S.L., Stroeve, J., & Box, J.E. (2005). Mapping daily snow/ice shortwave broadband albedo from

716   Moderate Resolution Imaging Spectroradiometer (MODIS): The improved direct retrieval

717   algorithm and validation with Greenland in situ measurement. *Journal of Geophysical*

718   *Research-Atmospheres, 110*

719 Liston, G.E., & Hiemstra, C.A. (2011). The Changing Cryosphere: Pan-Arctic Snow Trends (1979–

720   2009). *Journal of Climate, 24*, 5691-5712

721 López-Moreno, J.I., Valero-Garcés, B., Mark, B., Condom, T., Revuelto, J., Azorín-Molina, C., Bazo,

722   J., Frugone, M., Vicente-Serrano, S.M., & Alejo-Cochachin, J. (2017). Hydrological and

723   depositional processes associated with recent glacier recession in Yanamarey catchment,

724   Cordillera Blanca (Peru). *Science of the Total Environment, 579*, 272-282

725 Lyapustin, A., Wang, Y., Xiong, X., Meister, G., Platnick, S., Levy, R., Franz, B., Korkin, S., Hilker,

726   T., Tucker, J., Hall, F., Sellers, P., Wu, A., & Angal, A. (2014). Scientific impact of MODIS C5

727   calibration degradation and C6+ improvements. *Atmos. Meas. Tech., 7*, 4353-4365

728 Male, D.H., & Granger, R.J. (1981). Snow Surface-Energy Exchange. *Water Resources Research, 17*,

729   609-627

730 Malmros, J.K., Mernild, S.H., Wilson, R., Yde, J.C., & Fensholt, R. (2016). Glacier area changes in the

731   central Chilean and Argentinean Andes 1955-2013/14. *Journal of Glaciology, 62*, 391-401

732 Mann, H.B. (1945). Nonparametric Tests Against Trend. *Econometrica, 13*, 245-259

733 Marchane, A., Jarlan, L., Hanich, L., Boudhar, A., Gascoin, S., Tavernier, A., Filali, N., Le Page, M.,

734   Hagolle, O., & Berjamy, B. (2015). Assessment of daily MODIS snow cover products to

735   monitor snow cover dynamics over the Moroccan Atlas mountain range. *Remote Sensing of*

736   *Environment, 160*, 72-86

737 Masiokas, M.H., Christie, D.A., Le Quesne, C., Pitte, P., Ruiz, L., Villalba, R., Luckman, B.H.,

738   Berthier, E., Nussbaumer, S.U., González-Reyes, Á., McPhee, J., & Barcaza, G. (2016).

739   Reconstructing the annual mass balance of the Echaurren Norte glacier (Central Andes, 33.5° S)

740   using local and regional hydroclimatic data. *The Cryosphere, 10*, 927-940

741 Masiokas, M.H., Villalba, R., Luckman, B.H., Le Quesne, C., & Aravena, J.C. (2006). Snowpack

742   variations in the central Andes of Argentina and Chile, 1951-2005: Large-scale atmospheric

743   influences and implications for water resources in the region. *Journal of Climate, 19*, 6334-

744   6352

745 McClung, D.M. (2013). The effects of El Niño and La Niña on snow and avalanche patterns in British

746   Columbia, Canada, and central Chile. *Journal of Glaciology, 59*, 783-792

747   Mernild, S.H., Beckerman, A.P., Yde, J.C., Hanna, E., Malmros, J.K., Wilson, R., & Zemp, M.

748   (2015a). Mass loss and imbalance of glaciers along the Andes Cordillera to the sub-Antarctic

749   islands. *Global and Planetary Change, 133*, 109-119

750   Mernild, S. H., Liston, G. E., Hiemstra, C. A., Beckerman, A. P., Yde, J. C., and McPhee, J. (2016b).

751   The Andes Cordillera. Part IV: Spatiotemporal freshwater runoff distribution to adjacent seas

752   (1979– 2014). *International Journal of Climatology, 37(7)*, 3175–3196

753   Mernild, S. H., Liston, G. E., Hiemstra, C. A., Malmros, J. K., Yde, J. C., and McPhee, J. (2016a). The

754   Andes Cordillera. Part I: Snow Distribution, Properties, and Trends (1979–2014). *International*

755   *Journal of Climatology*, 37(4), 1680–1698

756   Mernild, S. H., Liston, G. E., Hiemstra, C. A., Yde, J. C., McPhee, J., and Malmros, J. K. (2016c). The

757   Andes Cordillera. Part II: Rio Olivares Basin Snow Conditions (1979–2014), Central Chile.

758   *International Journal of Climatology*, 37(4), 1699–1715.,

759   Mernild, S.H., Liston, G.G., Kane, D.L., Knudsen, N.F., & Hasholt, B. (2008). Snow, runoff, and mass

760   balance modeling for the entire Mittivakkat Glacier (1998-2006), Ammassalik Island, SE

761   Greenland. *Geografisk Tidsskrift-Danish Journal of Geography, 108*, 121-136

762   Mernild, S.H., Malmros, J.K., Yde, J.C., Wilson, R., Knudsen, N.T., Hanna, E., Fausto, R.S., & van

763   As, D. (2015b). Albedo decline on Greenland's Mittivakkat Gletscher in a warming climate.

764   *International Journal of Climatology, 35*, 2294-2307

765   Meza, F.J., Wilks, D.S., Gurovich, L., & Bambach, N. (2012). Impacts of Climate Change on Irrigated

766   Agriculture in the Maipo Basin, Chile: Reliability of Water Rights and Changes in the Demand

767   for Irrigation. *Journal of Water Resources Planning and Management, 138*, 421-430

768   Montecinos, A., & Aceituno, P. (2003). Seasonality of the ENSO-related rainfall variability in central

769   Chile and associated circulation anomalies. *Journal of Climate, 16*, 281-296

770   Moustafa, S.E., Rennermalm, A.K., Román, M.O., Wang, Z., Schaaf, C.B., Smith, L.C., Koenig, L.S.,

771   & Erb, A. (2017). Evaluation of satellite remote sensing albedo retrievals over the ablation area

772   of the southwestern Greenland ice sheet. *Remote Sensing of Environment, 198*, 115-125

773   Oerlemans, J., Giesen, R.H., & Van den Broeke, M.R. (2009). Retreating alpine glaciers: increased

774   melt rates due to accumulation of dust (Vadret da Morteratsch, Switzerland). *Journal of*

775   *Glaciology, 55*, 729-736

776 Neckel, N., Loibl, D., & Rankl, M. (2017). Recent slowdown and thinning of debris-covered glaciers in
777   south-eastern Tibet. *Earth and Planetary Science Letters, 464*, 95-102

778 Pellicciotti, F., Burlando, P., & Van Vliet, K. (2007). Recent trends in precipitation and streamflow in
779   the Aconcagua River basin, central Chile Glacier mass balance changes and meltwater
780   discharge. In, *Foz do Iguaçu*. International Association of Hydrological Sciences: IAHS

781 Peña, H., & Nazarala, B. (1987). Snowmelt-Runoff Simulation Model of a Central Chile Andean Basin
782   with Relevant Orographic Effects. In, *International Association of Hydrological Sciences*
783   *(IAHS)*. Vancouver, Canada: IAHS

784 Pfeffer, W.T., Arendt, A.A., Bliss, A., Bolch, T., Cogley, J.G., Gardner, A.S., Hagen, J.-O., Hock, R.,
785   Kaser, G., Kienholz, C., Miles, E.S., Moholdt, G., Mölg, N., Paul, F., Radi, Valentina, Rastner,
786   P., Raup, B.H., Rich, J., & Sharp, M.J. (2014). The Randolph Glacier Inventory: a globally
787   complete inventory of glaciers. *Journal of Glaciology, 60*, 537-552

788 Polk, M.H., Young, K.R., Baraer, M., Mark, B.G., McKenzie, J.M., Bury, J., & Carey, M. (2017).
789   Exploring hydrologic connections between tropical mountain wetlands and glacier recession in
790   Peru's Cordillera Blanca. *Applied Geography, 78*, 94-103

791 Prohaska, F. (1976). The climate of Argentina, Paraguay and Uruguay. In W. Schwerdfeger (Ed.),
792   *World Survey of Climatology* (pp. 13 - 112). New York: Elesevier

793 Ragettli, S., Immerzeel, W.W., & Pellicciotti, F. (2016). Contrasting climate change impact on river
794   flows from high-altitude catchments in the Himalayan and Andes Mountains. *Proceedings of*
795   *the National Academy of Sciences of the United States of America, 113*, 9222-9227

796 Riggs, G.A., Hall, D.K. & Román, M.O. (2017) Overview of NASA's MODIS and Visible Infrared
797   Imaging Radiometer Suite (VIIRS) snow-cover Earth System Data Records. *Earth Syst. Sci.*
798   *Data, 9,* 765-777.

799 Rittger, K., Painter, T.H., & Dozier, J. (2013). Assessment of methods for mapping snow cover from
800   MODIS. *Advances in Water Resources, 51*, 367-380

801 Rutllant, J., & Fuenzalida, H. (1991). Synoptic Aspects of the Central Chile Rainfall Variability
802   Associated with the Southern Oscillation. *International Journal of Climatology, 11*, 63-76

803 Saavedra, F.A., Kampf, S.K., Fassnacht, S.R., & Sibold, J.S. (2016). A snow climatology of the Andes
804   Mountains from MODIS snow cover data. *International Journal of Climatology*

805   Saavedra1, F.A., Kampf, S.k., Fassnacht, S.R., and Sibold, J.S. Changes in Andes Mountains snow
806   cover from MODIS data 2000-2014. *The Cryosphere Discuss.,* https://doi.org/10.5194/tc-2017-
807   72, in review, 2017.

808   Savitzky, A., & Golay, M.J.E. (1964). Smoothing and Differentiation of Data by Simplified Least
809   Squares Procedures. *Analytical Chemistry, 36*, 1627-1639

810   Sirguey, P., Still, H., Cullen, N.J., Dumont, M., Arnaud, Y., & Conway, J.P. (2016). Reconstructing the
811   mass balance of Brewster Glacier, New Zealand, using MODIS-derived glacier-wide albedo.
812   *The Cryosphere, 10*, 2465-2484

813   Sorman, A.U., Akyurek, Z., Sensoy, A., Sorman, A.A., & Tekeli, A.E. (2007). Commentary on
814   comparison of MODIS snow cover and albedo products with ground observations over the
815   mountainous terrain of Turkey. *Hydrology and Earth System Sciences, 11*, 1353-1360

816   Tedesco, M., Fettweis, X., Mote, T., Wahr, J., Alexander, P., Box, J.E., & Wouters, B. (2013).
817   Evidence and analysis of 2012 Greenland records from spaceborne observations, a regional
818   climate model and reanalysis data. *The Cryosphere, 7*, 615-630

819   Tekeli, A.E., Akyürek, Z., Arda Şorman, A., Şensoy, A., & Ünal Şorman, A. (2005). Using MODIS
820   snow cover maps in modeling snowmelt runoff process in the eastern part of Turkey. *Remote*
821   *Sensing of Environment, 97*, 216-230

822   Vuille, M., Kaser, G., & Juen, I. (2008). Glacier mass balance variability in the Cordillera Blanca, Peru
823   and its relationship with climate and the large-scale circulation. *Global and Planetary Change,*
824   *62*, 14-28

825   Wang, Z., Schaaf, C.B., Strahler, A.H., Chopping, M.J., Román, M.O., Shuai, Y., Woodcock, C.E.,
826   Hollinger, D.Y., & Fitzjarrald, D.R. (2014). Evaluation of MODIS albedo product (MCD43A)
827   over grassland, agriculture and forest surface types during dormant and snow-covered periods.
828   *Remote Sensing of Environment, 140*, 60-77

829   Warren, S.G., & Wiscombe, W.J. (1980). A Model for the Spectral Albedo of Snow. II: Snow
830   Containing Atmospheric Aerosols. *Journal of the Atmospheric Sciences, 37*, 2734-2745

831   Wilson, R., Mernild, S.H., Malmros, J.K., Bravo, C., & CarriÓN, D. (2016). Surface velocity
832   fluctuations for Glaciar Universidad, central Chile, between 1967 and 2015. *Journal of*
833   *Glaciology, 62*, 847-860

834   Wiscombe, W.J., & Warren, S.G. (1980). A Model for the Spectral Albedo of Snow. I: Pure Snow. *Journal of the Atmospheric Sciences, 37*, 2712-2733

836   Wolter, K., & Timlin, M.S. (2011). El Niño/Southern Oscillation behaviour since 1871 as diagnosed in an extended multivariate ENSO index (MEI.ext). *International Journal of Climatology, 31*, 1074-1087

839   Xu, W., Ma, H., Wu, D. & Yuan, W. (2017). Assessment of the Daily Cloud-Free MODIS Snow-Cover Product for Monitoring the Snow-Cover Phenology over the Qinghai-Tibetan Plateau. *Remote Sensing, 9,* 585.